Influence of ferrocyanide inhibitors on the transport and crystallization processes of sodium chloride in porous building materials

CRYSTAL GROWTH & DESIGN

Article

pubs.acs.org/crystal

Influence of Ferrocyanide Inhibitors on the Transport and Crystallization Processes of Sodium Chloride in Porous Building Materials

Sonia Gupta,[†] Kristina Terheiden,[†] Leo Pel,*[,†] and Alison Sawdy[‡]

[†]Transport in Permeable Media, Department of Applied Physics, Eindhoven University of Technology, P.O. Box 513, 5600 MB Eindhoven, The Netherlands

[‡]International Centre for the Study of the Preservation and Restoration of Cultural Property (ICCROM), Via di San Michele 13, 00153 Rome, Italy

ABSTRACT: Salt weathering leads to destruction of many valuable cultural heritage monuments and porous building materials. In order to reduce the impact of this, effective treatment methods are required. The use of crystallization inhibitors to mitigate salt damage has been proposed in the past; however, to date their effectiveness on cultural heritage objects has not been proven. Therefore a detailed experimental study to see the effect of crystallization inhibitors on the drying behavior of salinated porous materials has been undertaken. Two types of drying experiments were performed to observe the crystallization behavior of salt solutions with and without the presence of inhibitors: (1) in droplets of salt solution; (2) in porous supports (brick) contaminated with salt solution. From the droplet drying experiments it is shown that the presence of inhibitor results in higher supersaturation and changes the crystal morphology from cubic to dendritic crystals. In the brick drying experiments, due to the dendritic crystal morphology in the presence of inhibitor, advection becomes the governing phenomenon for ion transport. This results in the transport of salt ions to the outer surface of the brick, where crystallization results in the formation of nondestructive efflorescence. Meanwhile, inside the brick, higher supersaturation levels are not observed.

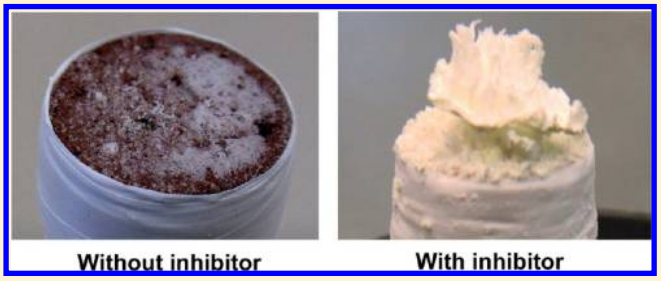

1. INTRODUCTION

Soluble salts such as chlorides, sulfates, and nitrates are widely recognized as a cause of destruction in porous building materials. The damage is mainly due to the crystallization of these soluble salts inside the porous matrix of these materials. The growth of salt crystals exerts pressure on the pore walls, which can exceed the tensile strength of the material thus leading to damage.[1] Therefore, an effective and practically feasible method is required in order to prevent or reduce this damage. Different methods have been proposed in the past such as controlling the environmental conditions,[2] or removal of salts from the substrate, for example, by dry brushing, water bath treatments, poulticing,[3] and electromigration[4] with varying degrees of success.

In light of the limited practical options available for the control of salt damage, the use of crystallization inhibitors has been proposed as a potential preventive treatment method. These inhibitors act either by preventing or delaying the onset of nucleation[5] (and hence crystallization) or by changing the crystal growth mechanism by adsorbing onto specific crystal faces.[6] Many applications of these inhibitors have been reported in different fields, including the use of polyacrylate for the prevention of crystallization of normal alkanes from diesel fuels,[7] polyphosphates and phosphates to control calcium carbonate and calcium sulfate scale formation and deposition[8] and also to prevent the spontaneous crystallization of gypsum.[9] However, their application in the field of architectural conservation is fairly new and not yet fully explored with very limited studies available.

Some authors have proposed the use of ferrocyanide (FC) ions as a preventive measure for NaCl crystallization as these compounds appear to promote the formation of nondestructive efflorescence rather than destructive subflorescence.[10,11] For bulk solutions, increased supersaturation levels in the presence of inhibitor have been reported in the past.[10] However, to our knowledge, to date no studies have been published regarding the effect of these compounds on the concentration of NaCl solutions inside a porous media. This indeed is a very important aspect for salt damage. It is known that the process behind the damage due to salt crystallization is the growth of salt crystals in confined spaces (e.g., pores), hence exerting crystallization pressure on the pore walls. However, for a salt crystal to grow in a confined space, a thin film of the liquid solution should be present surrounding the crystal[12] that can feed ions to the growing crystal. Also the growing crystal can only exert pressure if the salt solution layer in contact with the growing crystal is supersaturated. Thermodynamically the crystallization pressure

Received: February 16, 2012
Revised: May 25, 2012
Published: June 18, 2012

dx.doi.org/10.1021/cg3002288 | *Cryst. Growth Des.* 2012, 12, 3888−3898

can be related to supersaturation (C/C_o) of the solution by the well-known Corren's equation[13]

$$P_C = \frac{RT}{V_m} \ln \frac{C}{C_O} \quad (1)$$

where P_c is the crystallization pressure, R is the universal gas constant, T is the absolute temperature, V_m is the molar volume of the salt crystal, C and C_o are increasing concentration in vicinity of crystal and saturation concentration of NaCl respectively. The saturation concentration of NaCl is 6.1 m (i.e., 6.1 mol of NaCl/kg of water). Before using inhibitors to treat historic objects, detailed experimental studies are required to assess the effectiveness and safety of their application. In particular, it is important to understand their influence on crystallization behavior of NaCl, moisture, and ion transport, and also the development of salt damage in porous media. In this paper, we focus on the effect of hexa-cyanoferrate(II) inhibitor on the concentration levels reached by NaCl solutions within porous media during drying, and the associated water and ion transport processes taking place. This behavior is still not completely understood, because it is not easy to measure nondestructively the concentration of ions inside a porous material during dynamic experiments. Techniques like gravimetric analysis have been used for this type of analysis, but these have the disadvantages of being destructive to the sample and have poor spatial resolution. However, with the help of a specially designed nuclear magnetic resonance setup,[14] we were able to nondestructively measure both hydrogen and sodium ions simultaneously during drying experiments. Two types of drying experiments were performed: the first series on droplets of salt solution with and without inhibitor; and the second on porous materials contaminated with salt solution with and without inhibitor.

2. THEORETICAL BACKGROUND: MOISTURE AND ION TRANSPORT

When a wet porous material starts to dry due to evaporation, a moisture flow is induced within the porous material. If there are dissolved salt ions present, the moisture flow will carry the salt ions along with it toward the drying surface (advection). This leads to an accumulation of salt ions near the surface, thus increasing the local salt concentration in this region. Therefore, a peak in the salt concentration profile is observed near the drying surface of the material, which also explains why salt crystallization is first observed near the material surface. This surface accumulation also induces a concentration gradient within the material, which in turn induces diffusion to level off the gradient. Therefore there is a competition between advection that transports ions toward the surface and diffusion that will try to level off the concentration gradient (see Figure 1). For ion transport the molar flux J (mol m^{-2} s^{-1}) is given as[15]

$$J = C_f\theta\left(CU - D\frac{\partial C}{\partial x}\right) \quad (2)$$

Here the concentration C is given in mol l^{-1} instead of mol m^{-3}; therefore the term C_f is used as correction factor and its value is equal to 10^3, θ (m^3 m^{-3}) is the moisture content, D (m^2 s^{-1}) is the diffusion of salt ions in porous material given as $D = T^*D_{bulk}$, where T^* is the tortuosity and D_{bulk} is the bulk diffusion coefficient of salt ions, t (s) is the time, x (m) is the position, and U (m s^{-1}) is the fluid velocity. The change in salt content can be calculated using law of mass conservation as

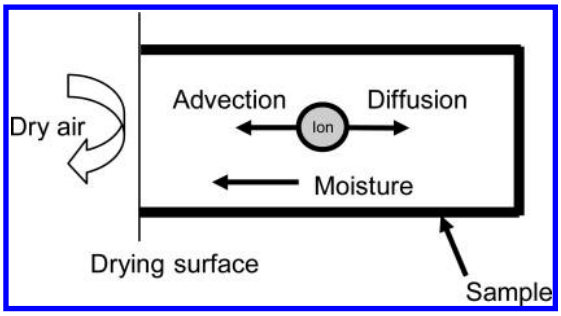

Figure 1. A schematic of one-dimensional drying of a sample saturated with salt solution.

$$C_f\frac{\partial C\theta}{\partial t} = -\frac{\partial J}{\partial x} \quad (3)$$

Combining eqs 2 and 3 the ion transport is given by following advection diffusion equation[16]

$$\frac{\partial C\theta}{\partial t} = \frac{\partial}{\partial x}\left[\theta\left(D\frac{\partial C}{\partial x} - CU\right)\right] \quad (4)$$

This equation shows the competition between advection and diffusion. On the right-hand side of the equation the first term represents the diffusion process, whereas the other term represents the advection process. The competition between these two processes is given by the Peclet number (P_e)[17]

$$P_e = \frac{|U|L}{D} \quad (5)$$

where L (m) is the length of the sample, and D was taken equal to 1.3×10^{-9} m^2 s^{-1}.[18] Using measured moisture profiles the fluid velocity can be calculated.[3] For $P_e < 1$, diffusion dominates and for $P_e > 1$, advection dominates.

3. EXPERIMENTAL SECTION

3.1. Materials. The materials used in this study were fired-clay brick and Granada limestone. The red fired-clay brick is of a type typically used for construction in The Netherlands and had an average porosity (as measured by water immersion method) of 0.32 m^3 m^{-3}, and a pore size distribution ranging from 1 to 10 μm (accounting for ~80% of the total pore space), as determined by mercury intrusion porosimetry (MIP) (see Figure 2). The Granada limestone is a buff colored stone commonly used as a building material in Granada, Spain. In this stone calcite is the main component (90 wt %), together with lesser amounts of SiO_2 and Al_2O_3.[19] This material has an average porosity (as measured by water immersion method) of 0.29 m^3 m^{-3}, and a bimodal pore size distribution with pores ranging from 0.3 to 1 μm (40%) and 1−100 μm (60%) as determined by MIP shown in Figure 2. In these experiments potassium hexa-cyanoferrate(II) trihydrate $K_4[Fe(CN)_6]\cdot 3H_2O$ was tested as a crystallization inhibitor. The active species in this chemical is hexa-cyanoferrate(II).[10] In addition to its function as crystallization inhibitor, hexa-cyanoferrate-(II) is also well-known commercially as an anticaking agent.[20]

3.2. Methods. *Drying of Salt Solution Droplets.* A series of drying experiments to observe the crystallization behavior of NaCl salt solution droplets with and without a crystallization inhibitor were undertaken. A schematic of the set up is shown in Figure 3. A cylindrical polymethyl methacrylate (PMMA) sample holder with an inner diameter of 20 mm was used. Droplets of 300 μL salt solution (3 m NaCl) with and without inhibitor were dried using 0% relative humidity and about 1 L min^{-1} air flow rate. Time lapse microscopy of the crystallization was performed using a dino-lite digital microscope,

dx.doi.org/10.1021/cg3002288 | Cryst. Growth Des. 2012, 12, 3888−3898

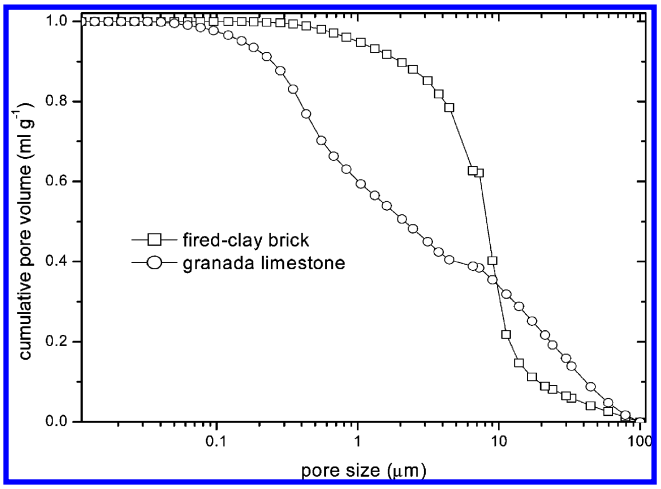

Figure 2. The cumulative pore size distribution of fired-clay brick and Granada limestone as measured by mercury intrusion porosimetry.

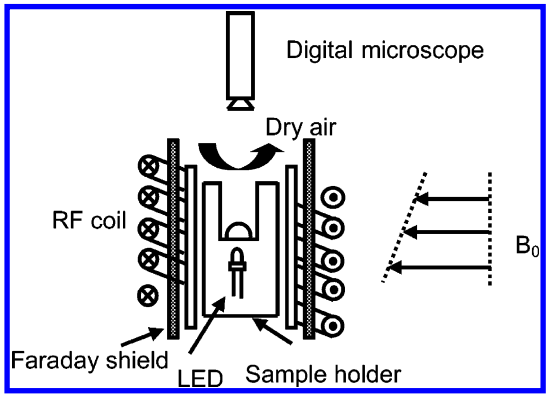

Figure 3. A schematic diagram of the NMR setup used for droplet drying experiments.

with four LEDs placed below the substrate as a lighting source for imaging within the NMR setup. The capture of photomicrograph images along with the NMR measurements gives the possibility to visualize the drying of the droplet while simultaneously obtaining information about NaCl concentration of the droplets.

Drying of Porous Building Materials Saturated with Salt Solution. A schematic diagram of the set up is given in Figure 4. The cylindrical samples 20 mm in diameter and 40 mm in length were saturated by capillary rise with salt solution (3 m NaCl) containing different concentrations of inhibitor (0.001 and 0.01 m). These samples were sealed using Teflon tape on all sides except the top surface and placed in the NMR sample chamber where they were exposed to dry air with a flow 1 L min^{-1} and 0% relative humidity, thereby creating a one-dimensional drying experiment. The sample position was moved in the vertical direction using a step motor to allow measurement of the moisture and Na content throughout the sample length. Measuring one drying profile takes about 3 h, while the complete drying experiment takes on the order of a few days depending on the composition of the salt solution. Therefore, small variations in the moisture and ion profiles during a single scan can be neglected. After each drying experiment was completed the efflorescence formed on the top of the sample was collected and weighed.

3.3. Nuclear Magnetic Resonance (NMR). In this study nuclear magnetic resonance (NMR) is used for carrying out nondestructive, quantitative, and simultaneous measurement of both the hydrogen and sodium ion content in the sample. NMR is based on the principle that in a magnetic field, nuclei have a specific resonance frequency and can be excited by a radio frequency field. The resonance frequency f (Hz) depends linearly on the magnitude of the magnetic field:

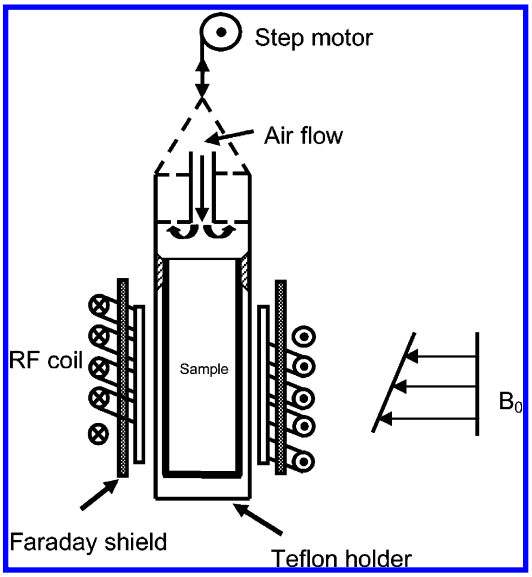

Figure 4. A schematic diagram of the NMR setup used for the brick drying experiments.

$$f = \frac{\gamma}{2\pi} B_o \tag{6}$$

where $\gamma/2\pi$ (Hz T^{-1}) is the gyro magnetic ratio, B_o (T) is the main magnetic field. For ^{1}H $\gamma/2\pi$ is 42.58 MHz T^{-1} and ^{23}Na is 11.26 MHz T^{-1}. Therefore, by using a specific frequency the method can be made sensitive to a particular type of nucleus, in this case either hydrogen or sodium. The signal intensity S of a spin echo as used in the experiment is given by

$$S = k\rho\left[1 - \exp\left(-\frac{T_r}{T_1}\right)\exp\left(-\frac{T_e}{T_2}\right)\right] \tag{7}$$

where S is the signal intensity, k is the sensitivity of the nuclei relative to hydrogen, ρ is the density of the nuclei, T_r and T_1 are the repetition time of the pulse sequence and spin−lattice relaxation time, T_e and T_2 are the spin echo time and spin−spin relaxation time. To measure the maximum signal, that is, from all pore sizes, T_e should be as short as possible as T_1 and T_2 are proportional to pore size. As the sensitivity of ^{23}Na nuclei is low relative to hydrogen (k_H = 1, k_{Na} = 0.1), 256 averages of the spin echo measurements are taken for Na nuclei relative to eight averages of hydrogen to achieve a sufficient signal-to-noise ratio. In our experiments the T_e used is 250 and 450 μs for H and Na respectively. Since the relaxation time for Na in NaCl crystals is on the order of 10 μs,[21] only dissolved Na ions are measured using the NMR set up. For the experiments presented here, a home-built NMR scanner with a static magnetic field of 0.78 T and gradient up to 0.3 T/m was used.[14] In order to perform quantitative measurements a Faraday shield was placed between the coil and the sample.[14]

4. RESULTS AND DISCUSSION

4.1. Droplet Drying Experiments. *Drying of Salt Solution Droplet without Inhibitor.* Initially we started with the drying of a 3 m salt solution droplet without inhibitor. The measured sodium and hydrogen content of the droplet is given in Figure 5a, whereas the calculated salt concentration is given in Figure 5b. As can be seen, as soon as drying has started the moisture content decreases, whereas the dissolved sodium content remains constant (see Figure 5a) and as a result the concentration in the droplet (Figure 5b) increases. After about 8 h a decrease in the sodium content is seen, indicating crystallization. This onset of crystallization was also observed by direct visualization (see picture) where cubic structured crystals

dx.doi.org/10.1021/cg3002288 | Cryst. Growth Des. 2012, 12, 3888−3898

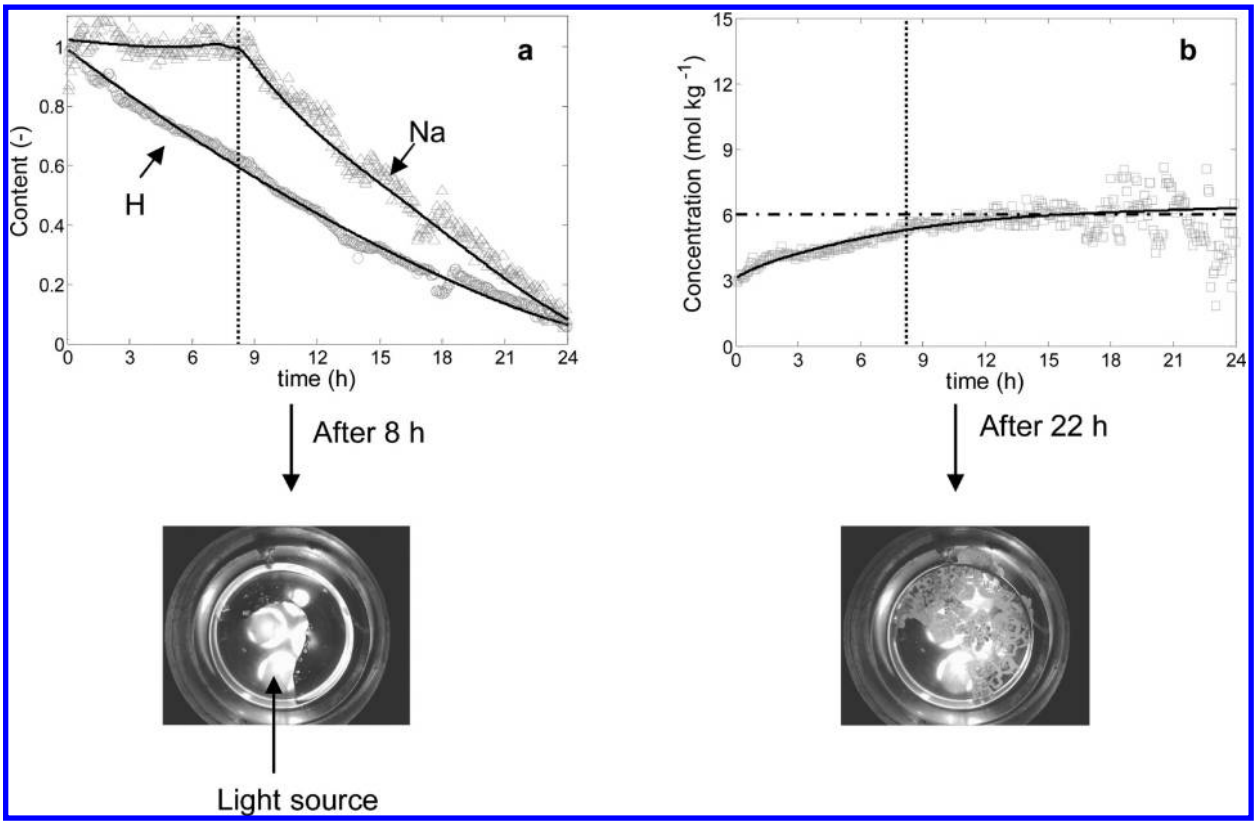

Figure 5. Drying of a 300 μL of 3 m NaCl salt solution droplet without inhibitor. (a) The measured normalized moisture (H) content (○) and normalized sodium (Na) content (△). (b) Calculated NaCl concentration (□) plotted as function of time. The pictures show the crystal morphology at the onset of crystallization (~8 h) and at the end of the experiment (~22 h).

were seen in the droplet. Also during drying the retraction of contact line was seen. This retraction of the droplet can decrease the effect of advection thereby reducing the concentration gradients in the drop, resulting in a homogeneous distribution of the ions in the droplet. This can also be verified by estimating the Peclet number and is discussed in the next section. Toward the end of the drying, the decrease in H and Na signals leads to an increase in noise in concentration. Cubic crystals are seen at the end of the experiment (see picture).

Analysis of Advection–Diffusion Processes in a Droplet. In order to do the analyses of the advection–diffusion processes in a droplet, the data are plotted in a way that is somewhat similar to a so-called efflorescence pathway diagram (EPD).[22] In the case of a droplet drying, the total amount of dissolved salt content in the droplet is plotted as a function of the normalized volume of the droplet ($V/V_{initial}$) and is given in Figure 6. In this diagram the competition between advection and diffusion can be shown in terms of the P_e number on the microscopic scale (i.e., on the length scale of the droplet). Two extreme situations can be distinguished. In the first case if diffusion dominates ($P_e < 1$) it will result in homogeneous distribution of ions throughout the droplet. Hence during drying the volume of the droplet will decrease and the concentration will increase homogenously throughout, until the saturation concentration of 6.1 m is achieved. From this moment onward any further drying will cause crystallization and the concentration would stay constant at 6.1 m. In the second case, if advection dominates ($P_e > 1$), it will result in concentration gradients in the droplet; for example, convective flow of the ions toward the periphery resulting in crystallization patterns somewhat similar

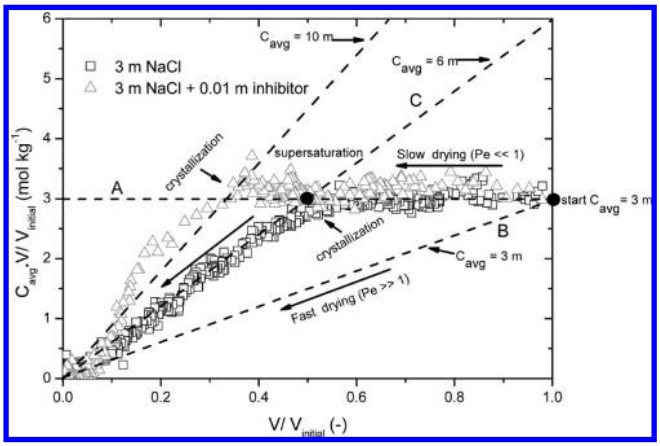

Figure 6. Advection–diffusion analysis diagram for the droplet drying experiment: The total amount of dissolved sodium in the droplet is plotted as a function of the volume of the droplet (V). Both the axes are normalized with respect to the initial volume of the droplet ($V_{initial}$). The division of both the axes gives the average concentration (C_{avg}) of Na in NaCl solution droplet shown by solid lines in the figure. The results for 3 m NaCl salt solution droplet with (△) and without inhibitor (□) are shown.

to a coffee-stain effect will be expected. In this case as soon as the volume of the droplet decreases and if there are enough nucleation sites (e.g., near periphery), immediate crystallization of salt will occur; that is, the total amount of dissolved salt will decrease. Therefore, in this case the concentration of dissolved salt ions inside the droplet will remain almost constant. In Figure 6 the data for the 3 m NaCl salt solution droplet are

dx.doi.org/10.1021/cg3002288 | *Cryst. Growth Des.* 2012, 12, 3888–3898

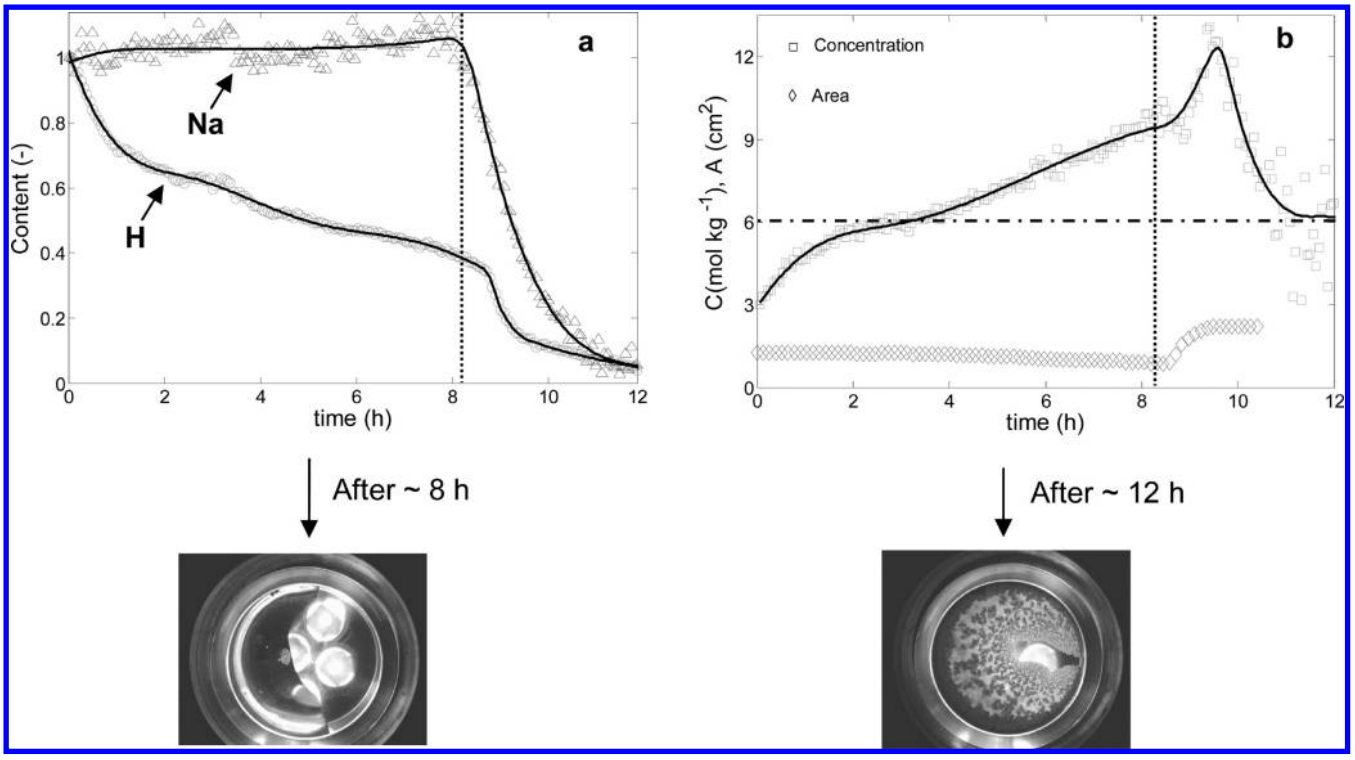

Figure 7. Drying of a 300 μL of 3 m NaCl salt solution droplet with 0.01 m inhibitor. (a) The measured normalized moisture (H) content (○) and normalized sodium (Na) content (△). (b) Calculated NaCl concentration (□) and area of the droplet (◊) plotted as function of time. The pictures show the crystal morphology at the onset of crystallization (~8 h) and at the end of the experiment (~12 h).

plotted. As can be seen for the salt solution droplet, initially the $P_e < 1$ path is followed indicating diffusion dominance and the concentration increased until nearly the saturation concentration was reached, after which it stayed constant at approximately the saturation concentration 6.1 m.

Drying of Salt Solution Droplet with Inhibitor. Next the drying of 3 m NaCl droplet in the presence of 0.01 m inhibitor was studied. In Figure 7a the measured sodium and hydrogen signals are given as function of time, whereas in Figure 7b the corresponding calculated concentration is given. In the presence of inhibitor, during approximately the first 1.5 h a faster drying rate was observed. During this time the moisture content decreases and sodium content remains constant, thereby resulting in an increase in solution concentration. After approximately 2 h the concentration in the droplet was on the order of 6.1 m but no crystallization was observed. As the drying progresses the concentration increased and the system supersaturated slowly. In Figure 7b we have also plotted the surface area of the droplet. As can be seen due to evaporation the surface area of the droplet decreased continuously. After ~8 h a faster decrease in moisture and sodium content was observed indicating crystallization. This was also observed by direct visualization (see picture). A small bunch of dendritic crystals were observed near the edge of the droplet. The corresponding average concentration at this point was nearly 10 m giving a supersaturation of 1.6 (calculated as C/C_o). From this moment onward the average concentration in the droplet continued to increase as a rapid increase in the surface area of the droplet was observed. This was due to the formation of dendritic crystals, the branches of which provided a pathway for the solution to spread over a much larger surface area, this phenomenon being commonly known as "salt creep" (see also Figure 7). Because of the enlarged surface area for evaporation a similar increase in the drying rate was observed, and the solution concentration increased to nearly 12 m. After about 9.5 h the drying rate decreased and no further spreading of the droplets was observed. Meanwhile, the concentration returned to the equilibrium concentration (6.1 m).

The results from the drying of a salt solution droplet with inhibitor are also plotted in Figure 6; as can be seen in this case the sodium concentration also remains homogeneous until crystallization and the droplet supersaturates, reaching a maximum concentration on the order of 10 m before crystallization. These results show that the ferrocyanide is acting as a strong nucleation inhibitor, which delays the onset of crystallization resulting in higher solution concentration. The inhibitor's presence also changes the NaCl crystal morphology. The mechanism of the inhibitor action on NaCl nucleation and growth has been studied in detail by Navarro and co-workers.[10]

4.2. Brick Drying Experiments. In the previous section we have shown that the presence of an inhibitor significantly increases the supersaturation within salt solution droplets. This delay in onset of crystallization can promote efflorescence growth by inhibiting NaCl nucleation inside the stone. Also this delay may be an advantage in situations where the object is exposed to a fluctuating environment. For such a case, the conditions for the crystallization may only be temporarily met. Nevertheless when exposed for periods of sustained low RH the critical supersaturation of the NaCl solution may be reached. As explained earlier higher supersaturation can cause higher crystallization pressure and hence the risk of damage is then greater. Therefore to ascertain the effects of the ferrocyanide inhibitor on the ion transport and crystallization behavior of sodium chloride solution within porous media a series of one-dimensional drying experiments were performed using fired-clay brick and Granada limestone substrates.

dx.doi.org/10.1021/cg3002288 | *Cryst. Growth Des.* 2012, 12, 3888−3898

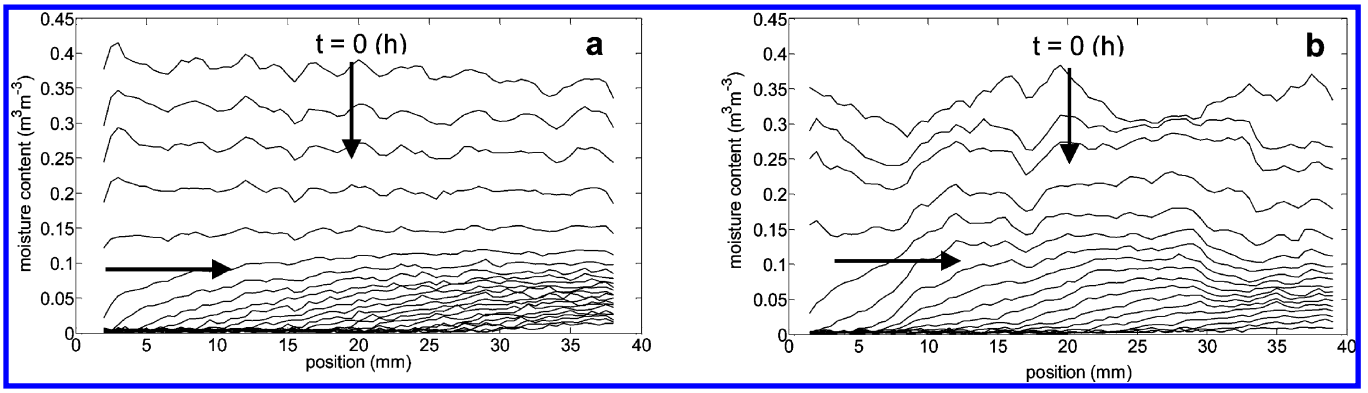

Figure 8. The measured moisture profiles for (a) fired-clay brick and (b) Granada limestone plotted as a function of position during drying. The profiles are given for every 3 h. The samples were initially capillary saturated with water and dried using dry air with flow 1 L min^{-1} and 0% relative humidity. The drying surface is at 0 mm. The vertical arrow shows the homogeneous drying of the sample and the horizontal arrow shows the penetration of the receding drying front.

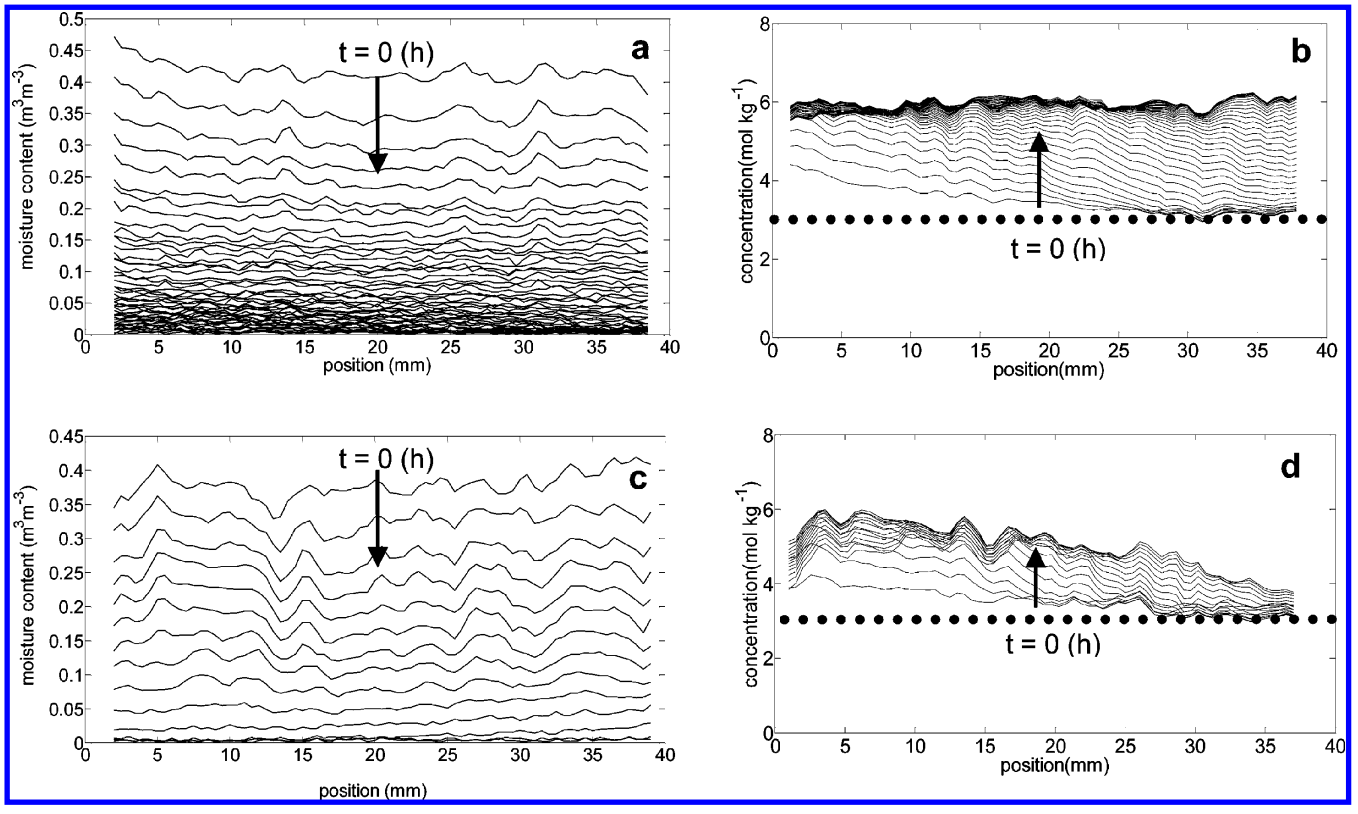

Figure 9. The measured moisture profiles (a) and the corresponding concentration profiles (b) for fired-clay brick, and the measured moisture profiles (c) and the corresponding concentration profiles (d) for Granada limestone, plotted as a function of position during drying. These samples were initially capillary saturated with 3 m NaCl solution and dried using dry air with flow 1 L min^{-1} and 0% relative humidity. The profiles are given for every 3 h. The drying surface is at 0 mm. Efflorescence up to ~7% and ~10% was seen on the surface of the fired-clay brick and Granada limestone respectively.

Drying of Samples Saturated with Pure Water. First, the drying behavior of fired-clay brick and Granada limestone capillary saturated with pure water was studied. The measured moisture profiles for both porous materials during the drying process are given in Figure 8. Some recurrent irregularities can be seen in the profiles, for example, at ~20 mm in both the fired-clay brick and the Granada limestone. These variations are most likely to be the result of inhomogeneities of the sample. For both materials, two drying stages can be observed, that is, externally limited and internally limited. The first 3−4 profiles in both samples are almost flat representing the first externally limited drying stage (shown by a vertical arrow in Figure 8a,b). During this stage there is continuous capillary flow of water to the surface and drying is limited by external conditions such as relative humidity and air flow. Afterward, the drying front starts to recede below the sample surface, and the moisture profiles are no longer flat (shown by a horizontal arrow in Figure 8a,b). This represents the second internally limited drying stage where the continuous capillary network of water breaks up to form liquid islands. During this stage drying occurs by vapor diffusion through the porous medium, in response to the relative humidity gradient between the vicinity of the liquid

dx.doi.org/10.1021/cg3002288 | *Cryst. Growth Des.* 2012, 12, 3888−3898

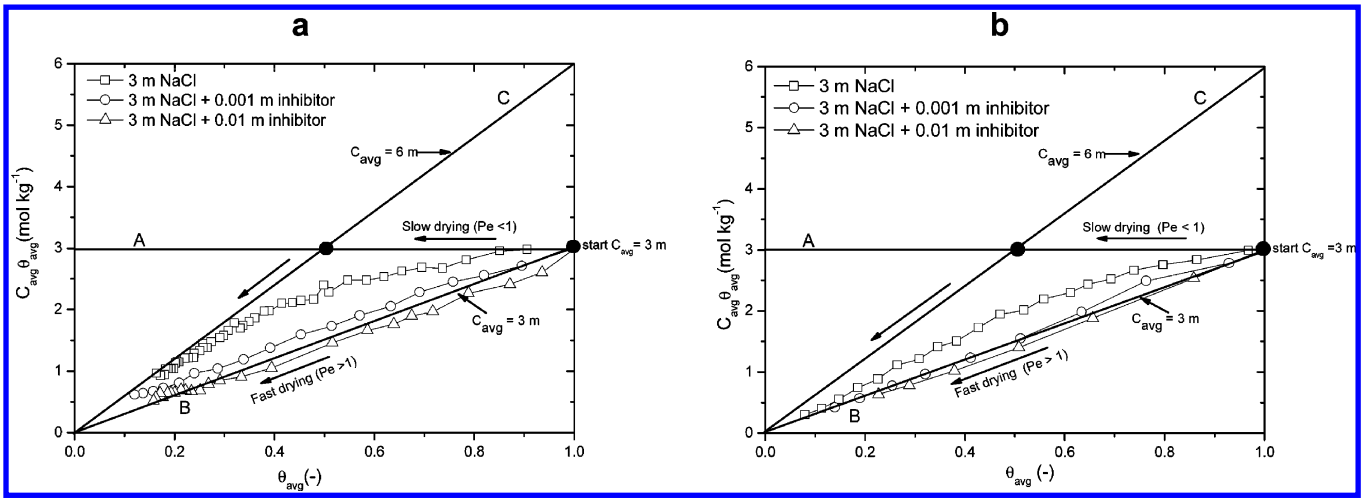

Figure 10. Efflorescence pathway diagram for the brick drying experiment: The total amount of dissolved sodium content is plotted as a function of time dependent average moisture content (θ_{avg}) in the brick. Both the axes are normalized with respect to the initial average moisture content. The division of both the axes gives the average concentration (C_{avg}) of Na in the brick as shown by solid lines in the figure. The results are shown for (a) fired-clay brick and (b) Granada limestone. The materials were capillary saturated with 3 m NaCl solution without and with (0.001 and 0.01 m) inhibitor.

island and the external drying surface of the material.[23] The transition point between these two drying stages can be identified as the critical moisture content. In the case of fired-clay brick and Granada limestone, the critical moisture content was observed to be near 0.1 m^3 m^{-3} and 0.12 m^3 m^{-3} respectively.

Drying of Samples Saturated with 3 m NaCl Solution. To study the effect of salt on the drying behavior, the samples were capillary saturated with salt solution. The measured moisture profiles and the calculated concentration profiles for the fired-clay brick are given in Figure 9a,b and for Granada limestone in Figure 9c,d. The dotted line in the concentration profiles (Figure 9b,d) is a reference line showing the initial solution concentration (3 m). For both samples, the presence of salt slows down the drying relative to water loaded samples. For example, fired-clay brick saturated with salt solution took 10−11 days to dry in comparison to only 4−5 days for the water saturated bricks. This difference in behavior can be explained by looking at the boundary conditions as given by

$$q_v = \frac{\beta}{\rho}(h_a - h_{al}) \tag{8}$$

where q_v (m^3 m^{-2} s^{-1}) is the vapor flux at the air/material interface, β (mol m^{-2} s^{-1}) is the mass transfer coefficient, ρ (mol m^{-3}) is the molar density of liquid water, h_a is the partial pressure of water vapor in the surrounding, and h_{al} is the partial pressure of water vapor at the air/material interface.

In the case of water saturated samples, the air in direct contact with water at the material/air interface is saturated with water vapor. The corresponding relative humidity is 100%. If there is a relative humidity gradient between the interface and the surrounding, the water vapor moves away from the surface, thereby causing drying of the material. However, the presence of salt lowers the saturated water vapor pressure due to solute solvent interaction. Therefore the local relative humidity at the air/material interface becomes less than 100% (for saturated NaCl 75%). This in turn reduces the relative humidity gradient,[23] thereby causing slower drying of the salt saturated samples. During drying an increase in concentration was seen (see Figure 9b,d) near the drying surface indicating advection of ions toward the top. Using the measured moisture profiles the fluid velocity was calculated and the corresponding P_e number was determined.[3] $P_e \sim 4$ in fired-clay brick and $P_e \sim 6$ in Granada limestone confirms advection is dominant. Because advection salt ions accumulate near the drying surface, when this salt ion accumulation exceeds the saturation concentration crystallization will occur. These salt crystals can block the pores near the drying surface. Especially for fired-clay brick which has smaller pores the effect of blockage is seen on the drying rate. As the moisture content approaches 0.1 m^3 m^{-3}, the drying slows down to such an extent that diffusion dominates, and the salt concentration starts to level off. We found in this case $P_e \sim$ 0.8. However, in Granada limestone the blockage effect was not seen due to the presence of bigger pores. No leveling off of the concentration was seen in Granada limestone during the experiment and the Peclet number remained greater than one.

Also, no receding drying front was observed in the case of salt saturated samples in contrast to water saturated samples. The slower drying rate and change in the wetting properties of the solution in the presence of NaCl might be responsible for this.[21] The efflorescence formed on the surface was collected at the end of the experiment and weighed to calculate the amount of salt coming out of the sample. Approximately 7% and 10% of the initial salt content came out of the fired-clay brick and Granada limestone respectively.

Efflorescence Pathway Diagram (EPD). To understand the crystallization processes during brick drying, the data were plotted on a so-called efflorescence pathway diagram (EPD).[22] In this case we have calculated the Peclet number on the macroscopic scale, that is, on the length scale of the brick. The dissolved salt content is plotted as a function of normalized moisture content of the brick. The EPDs for both drying experiments are given in Figure 10. As in the case of the droplet two extreme situations can be distinguished on this macroscopic scale. In the first case when the system dries very slowly ($P_e < 1$); diffusion dominates resulting in a homogeneous distribution of ions throughout the sample. For this situation, starting from an initial concentration of 3 m the salt solution concentration will increase throughout the sample, until the saturation concentration 6.1 m is achieved. From this moment

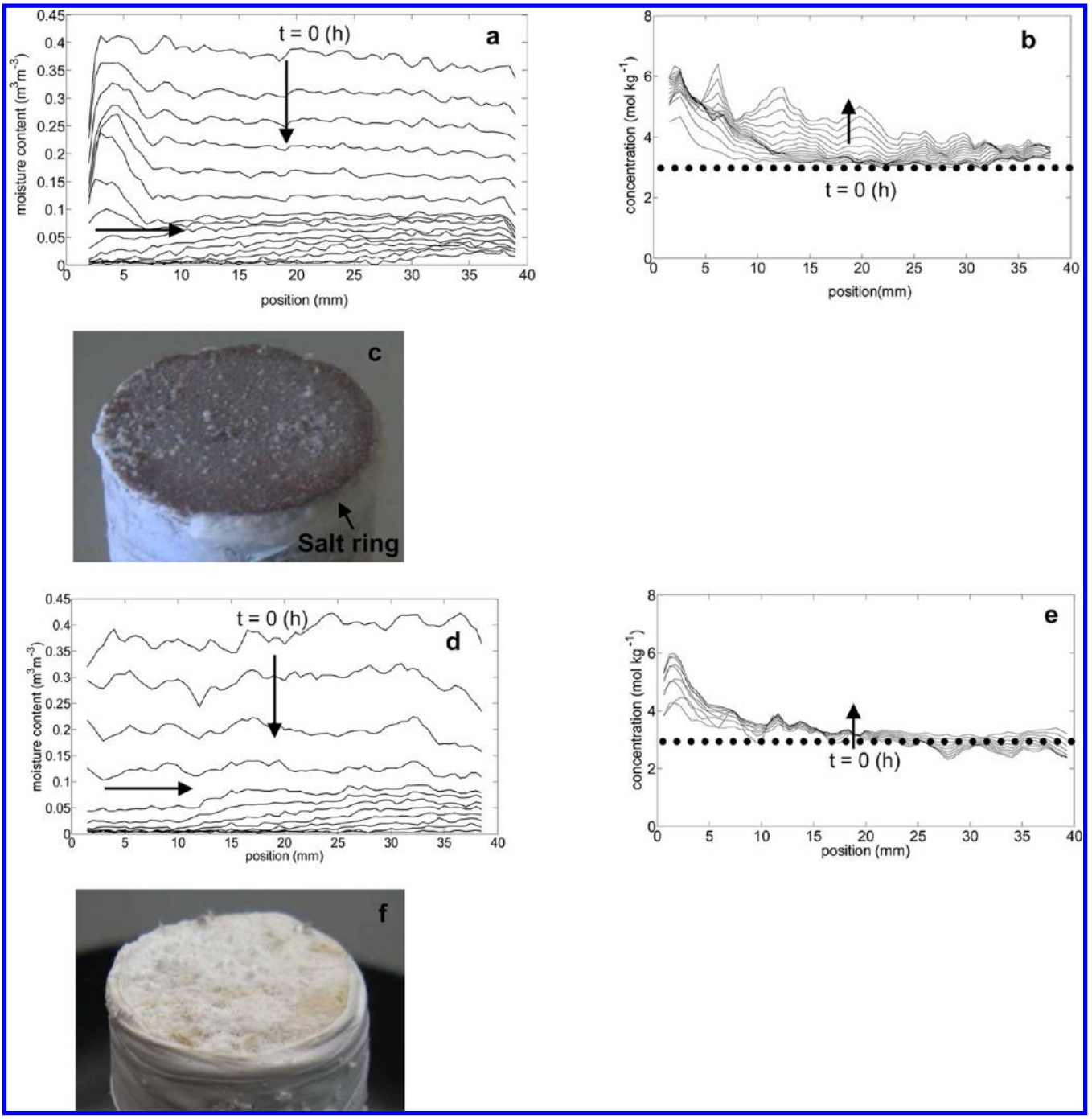

Figure 11. The measured moisture profiles (a), the corresponding concentration profiles (b), and the efflorescence seen at the end of the drying on the surface of the sample (c) for fired-clay brick; and the measured moisture profiles (d), the corresponding concentration profiles (e), and the efflorescence seen at the end of the drying on the surface of the sample (f) for Granada limestone, plotted as a function of position during drying. These samples were initially capillary saturated with 3 m NaCl solution + 0.001 m inhibitor and dried using dry air with flow 1 L min^{-1} and 0% relative humidity. The profiles are given for every 3 h. The drying surface is at 0 mm.

onward any further drying will cause crystallization. Furthermore, the concentration will stay constant at 6.1 m. In the second case the system dries very fast (P_e > 1), that is, advection dominates. In this case, ions will be transported along with the moisture flow toward the drying surface. Thus, the concentration will increase near the drying surface. If there are enough nucleation sites, accumulation of ions beyond the saturation concentration will immediately result in crystallization near the surface as efflorescence. Efflorescence preferentially occurs in the regions where the evaporation is fastest. It also acts as a porous network and increases the effective surface area for evaporation, thus causing higher evaporation flux.[18,24] Because of higher evaporation flux, the underlying velocities also increase and thereby pumping more dissolved salt ions toward the surface. In this way, efflorescence acts as a sink for the ions. If rate of crystallization (efflorescence) is high enough, the ratio of transported Na to hydrogen ions remains constant and the dissolved salt ion concentration (ratio of dissolved sodium to hydrogen ions)

dx.doi.org/10.1021/cg3002288 | *Cryst. Growth Des.* 2012, 12, 3888−3898

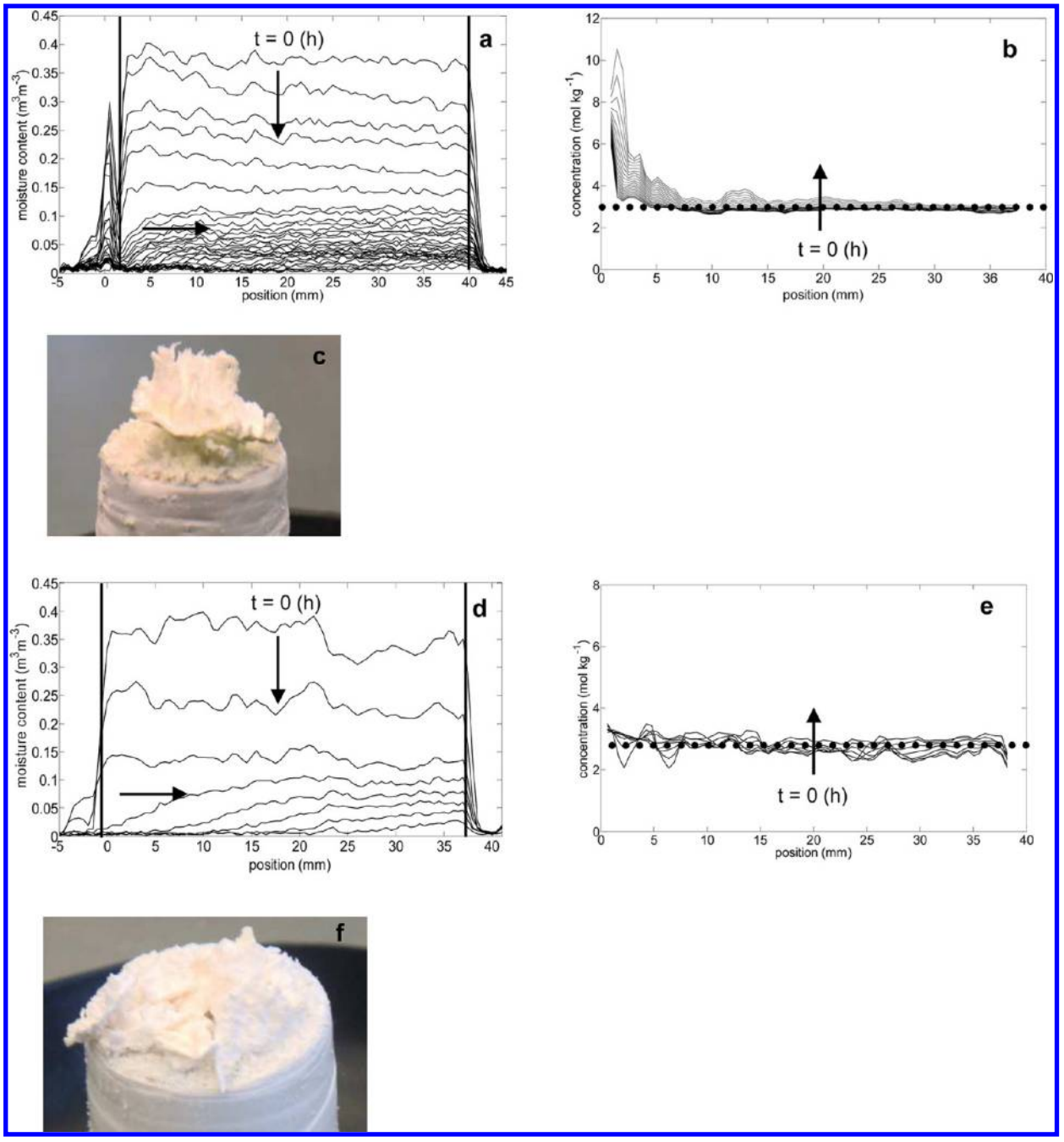

Figure 12. The measured moisture profiles (a), the corresponding concentration profiles (b), and the efflorescence seen at the end of the drying on the surface of the sample (c) for fired-clay brick; and the measured moisture profiles (d) the corresponding concentration profiles (e), and the efflorescence seen at the end of the drying on the surface of the sample (f) for Granada limestone, plotted as a function of position during drying. These samples were initially capillary saturated with 3 m NaCl solution + 0.01 m inhibitor and dried using dry air with flow 1 L min^{-1} and 0% relative humidity. The drying surface is at 0 mm. The vertical black bars indicate the sample boundary.

inside the material will remain almost constant at the initial concentration.

In the brick drying experiments, for the materials saturated with salt only a path in between the extreme cases (P_e < 1 and P_e > 1) is followed. For fired-clay brick after some time as the drying slows down the P_e < 1 path is followed. During this time the salt concentration levels off at ca. 6.1 m. For the Granada limestone, a path in between the two extreme situations is followed throughout the experiment and no leveling off of the concentration is seen due to the presence of bigger pores.

Drying of Samples Saturated with 3 m NaCl Solution + 0.001 m Inhibitor. In order to see the effect of inhibitor on the salt transport behavior and the concentration of ions inside the materials, samples were capillary saturated with 3 m salt solution mixed with 0.001 m inhibitor. The measured moisture profiles and the calculated concentration profiles for the fired-clay brick are given in Figure 11a,b and for Granada limestone are given in Figure 11d,e. In this case due to a somewhat noisy moisture measurement, a few local peaks are seen in the concentration profiles at the end of the drying experiment. Figure 11, panels c and f show the efflorescence seen at the end

dx.doi.org/10.1021/cg3002288 | *Cryst. Growth Des.* 2012, 12, 3888−3898

of drying on the surface of fired-clay brick and Granada limestone respectively. The drying of the materials saturated with salt solution + 0.001 m inhibitor was faster than the materials saturated with salt solution only. The concentration increases near the drying surface due to advection (see Figure 11b,e). The calculated value of $P_e \sim 10$ (as determined in section 2) in both cases confirms advection is the dominant phenomenon and causes salt crystallization near the drying surface. Because of dendritic crystal growth morphology in the presence of inhibitor, the effective surface area for evaporation increases. The salt solution creeps along the branches of the dendrites and transports more and more dissolved salt ions toward the drying surface which was seen as efflorescence by the end of the drying experiment. Also, the crystals were seen to form a salt ring around the material. Approximately 36% of salt in fired-clay brick and 47% of salt in limestone was deposited out of the sample as efflorescence. For fired-clay brick a distinct moisture peak starts building up near the drying surface. Initially this peak increases in height but afterward near the end of drying it starts to diminish. This peak was probably due to the presence of moisture in the salt ring formed around the material at nearly top 5 mm of the sample (see Figure 11a). As this outer salt ring was in the scanning region of the NMR, it also contributes to the signal. Therefore it is hard to draw a firm conclusion in the first few millimeters of the material. However, no supersaturation is seen inside the materials. In the presence of inhibitor a receding moisture front starts penetrating again near 0.08 $m^3\ m^{-3}$ in both the samples. This is probably due to faster drying and lower salt content inside the sample. These results are also plotted in the EPD (see Figure 10). For both the materials in the presence of the inhibitor the boundary line $P_e > 1$ is followed indicating faster drying compared to salt saturated samples and the concentration stays almost constant at around the starting concentration. A constant decrease in the dissolved sodium content is seen and advection is the governing process throughout the drying.

Drying of the Samples Saturated with 3 m NaCl Solution + 0.01 m Inhibitor. Next, the inhibitor concentration was increased by 10-fold. The measured moisture profiles and the corresponding calculated concentration profiles for fired-clay brick are shown in Figure 12a,b and for Granada limestone are shown in Figure 12d,e. The vertical black lines in Figure 12a,d indicate the sample boundaries. The drying surface is at 0 mm. We have also shown the moisture content outside the sample boundaries (see Figure 12a,d). Figure 12, panels c and f show the efflorescence seen at the end of drying experiment on the drying surface of fired-clay brick and Granada limestone respectively.

In the presence of 0.01 m inhibitor, for both fired-clay brick and Granada lime stone, drying was faster than the salt saturated samples. A distinct moisture peak was seen on the drying surface of the materials. This peak was probably due to the moisture present in the efflorescence found on the surface of material. In fired-clay brick, the salt concentration up to 10 m is seen near the drying surface (see Figure 12b). As discussed before, it is difficult to draw conclusions on the basis of the measured concentration in first few millimeters of the material. In rest of the material the concentration stays constant nearly at the starting concentration; that is, 3 m and no supersaturation was observed. In Granada limestone (see Figure 12e), the concentration remains nearly constant at the starting concentration and no supersaturation was observed. Approximately 69% of the salt in fired-clay brick and approximately 51% salt in limestone were deposited at the surface in the form of efflorescence. Here also a receding moisture front starts penetrating near 0.1 $m^3\ m^{-3}$ for both cases.

From these results it is concluded that in the presence of inhibitor the drying conditions near the material/air interface change due to the change in crystal morphology. The immediate crystallization near the drying surface provides a sink for the salt ions and as a result the concentration of the dissolved salt ions stays constant at the initial concentration inside the material.

5. CONCLUSIONS

From the droplet drying experiments it is concluded that the presence of inhibitor makes the drying process faster. Higher supersaturation and change in crystal morphology were observed. After attaining supersaturation the salt concentration returns to the equilibrium concentration (6.1 m). This clearly shows that the system goes from a metastable state to stable equilibrium state and NMR provides a sufficient signal-to-noise ratio to determine this transition. Besides this, a tremendous spreading of the salt crystals in the form of efflorescence was observed. This increase in efflorescence formation was related to the inhibitor concentration and resulted in elevating the drying rate.

From the brick drying experiments it is concluded that the presence of inhibitor changes the drying conditions near the material/air interface due to changes in crystal morphology. Dendrite crystals provide a much larger surface area for evaporation and advection becomes the governing phenomenon throughout the drying process. Advection of dissolved salt ions causes crystallization of salt near the drying surface as nondestructive efflorescence. As a result the concentration inside the material stays almost constant at the initial concentration. This indicates that ferrocyanide ions could potentially be effective against NaCl damage in building materials as they promote nondestructive efflorescence rather than destructive subflorescence.

At the same time there are many questions still to be addressed such as (a) the effect of varying environmental conditions on the inhibitor action and (b) the effect of the inhibitor on salt mixtures present in building materials, since in practice there is not only the single salt present in the building materials but indeed a mixture of salt is present.

AUTHOR INFORMATION

Corresponding Author

*Tel.: +31 40 247 3406. Fax: +31 40 243 2598. E-mail: l.pel@tue.nl. Internet: http://www.phys.tue.nl/nfcmr.

Notes

The authors declare no competing financial interest.

ACKNOWLEDGMENTS

We thank Hans Dalderop and Jef Noijen for their technical assistance. A part of this project is supported by the Dutch technology foundation (STW). Special thanks to Carlos Rodriguez Navarro for providing the Granada limestone for study.

REFERENCES

(1) Scherer, G. W. *Cem. Concr. Res.* **1999**, *29*, 1347−1358.
(2) Navarro, C. R.; Doehne, E. *Earth Surf. Process Landforms* **1999**, *24*, 191−209.

(3) Pel, L.; Sawdy, A.; Voronina, V. *J. Cult. Herit.* **2010**, *11*, 59−67.
(4) Ottosen, M. L.; Dalgaard, I. R. *Mater. Struct.* **2009**, *42*, 961−971.
(5) Sangwal, K. J. *Cryst. Growth* **1993**, *128*, 1236−1244.
(6) Sangwal, K. *Prog. Cryst. Growth Charact.* **1998**, *36*, 163−248.
(7) Hutter, J. I.; Hudson, S.; Smith, C.; Tetervak, A.; Zhang, J. J. *Cryst. Growth* **2004**, *273*, 292−302.
(8) Butt, F. H.; Rahman, F.; Baduruthamal, U. *Desalination* **1995**, *103*, 189−198.
(9) Hernandez, A.; Rocca, A.; Power, H.; Graupner, U.; Ziegenbalg, G. J. *Cryst. Growth* **2006**, *295*, 217−230.
(10) Navarro, C. R.; Fernandez, L. L.; Doehne, E.; Sebastian, E. J. *Cryst. Growth* **2002**, *243*, 503−516.
(11) Lubelli, B.; Van Hees, R. P. J. *J. Cult. Herit.* **2007**, *8*, 223−234.
(12) Taber, S. *Am. J. Sci.* **1916**, *41*, 532−556.
(13) Correns, W. *Disc.Faraday Soc.* **1949**, *5*, 267−271.
(14) Pel, L. Moisture Transport in porous building materials. Ph.D. thesis, Eindhoven University of Technology, The Netherlands, 1995.
(15) Bear, J.; Bachmat, Y. *Introduction to Modeling of Transport Phenomena in Porous Media*; Klumer: Dordrecht, The Netherlands, 1990; Vol. *4*.
(16) Wilke, C. R. *Diffusion in Gases and Liquids*; McGraw-Hill: London, 1988.
(17) Huinink, H. P.; Pel, L.; Michels, M.A. J. *Phys. Fluids* **2002**, *14*, 1389−1395.
(18) Veran-Tissoires, S.; Marcoux, M.; Prat, M. *Phys. Rev. Lett.* **2012**, *108*, 054502.
(19) Navarro, C. R.; Ruiz-Agudo, E. *Internal Report of European Project SALT CONTROL* (Project no. 501517 (Contract SSP1-CT-2003-501571)) (EU project no. 501571, prevention of salt damage to the built cultural heritage by the use of crystallization inhibitors).
(20) Van Damme-van Weele, I. M. A. Influence of additives on the growth and dissolution of sodium chloride crystals, Ph.D. thesis, Technical University Twente, The Netherlands, 1965.
(21) Pel, L.; Huinink, H.; Kopinga, K. *Magn. Reson. Imaging* **2003**, *21*, 317−320.
(22) Pel, L.; Huinink, H. P.; Kopinga, K. *Appl. Phys. Lett.* **2002**, *81*, 2893−2895.
(23) Hall, C.; Hoff, W. D. *Water Transp. in Brick, Stone and Concrete*; Spon Press: London, 2002; pp 188−194.
(24) Sghaler, N.; Prat, M. *Transp. Porous Med.* **2009**, *80*, 441−454.